International Journal of Modern Physics E
Vol. 27, No. 2 (2018) 1850010 (14 pages)

DOI: 10.1142/S0218301318500106

Incomplete mass transfer processes in ^{28}Si+^{93}Nb reaction

R. Tripathi*,‡, S. Sodaye*, K. Ramachandran†,
S. K. Sharma* and P. K. Pujari*

*Radiochemistry Division,
Bhabha Atomic Research Centre,
Mumbai 400085, India

†Nuclear Physics Division,
Bhabha Atomic Research Centre,
Mumbai 400085, India
‡rahult@barc.gov.in

Received 29 August 2017
Revised 5 January 2018
Accepted 13 January 2018
Published 14 February 2018

Cross sections of reaction products were measured in ^{28}Si+^{93}Nb reaction using recoil catcher technique involving by off-line gamma-ray spectrometry at beam energies of 105 and 155 MeV. At $E_{\rm lab} = 155$ MeV, the contribution from different incomplete mass transfer processes is investigated. Results of the present studies show the contribution from deep inelastic collision (DIC), massive transfer or incomplete fusion (ICF) and quasi-elastic transfer (QET). The contribution from massive transfer reactions was confirmed from the fractional yield of the reaction products in the forward catcher foil. The present results are different from those from the reactions with comparatively higher entrance channel mass asymmetry with lighter projectiles, for which dominant transfer processes are ICF and QET which involve mass transfer predominantly from projectile to target. The N/Z values of the products close to the target mass were observed to be in a wide range, starting from N/Z of the target (^{93}Nb) and extending slightly below the N/Z of the composite system, consistent with the contribution from DIC and QET reactions. At $E_{\rm lab} = 105$ MeV, a small contribution from QET was observed in addition to complete fusion.

Keywords: Incomplete fusion; transfer reactions; deep inelastic collisions; recoil catcher method; gamma-ray spectrometry.

PACS Number(s): 25.70.Hi, 25.70.−z

1. Introduction

Heavy ion fusion has been extensively investigated in the last few decades. These studies have revealed that, in the collision of two heavy nuclei, a number of processes involving incomplete mass transfer may occur in addition to complete fusion. These reactions can be categorized into quasi-elastic transfer (QET), massive transfer and

deep inelastic collision (DIC). Various mechanisms differ in terms of the energy and N/Z equilibration. QET reactions are least dissipative whereas DIC may involve complete equilibration of projectile energy with outgoing products appearing at energies corresponding to the exit channel Coulomb barrier. Incomplete fusion (ICF) or massive transfer reactions lie in between these two extreme regimes of energy and N/Z equilibration. Masses of the projectile-like fragments (PLFs) and their kinetic energy spectra and angular distributions give information about the contribution from different types of mechanisms.[1–3] QET involves transfer of a few nucleons with minimal energy dissipation. ICF or massive transfer reactions involve large mass transfer from lighter to heavier reaction partner. DIC involves mutual exchange of nucleons between the projectile and the target nuclei, leading to wings around projectile and target masses in the mass distribution. In addition to these reactions, there can be contribution from fission-like events involving unidirectional flow of the mass between projectile and target nuclei which is governed by the potential energy landscape. For reaction systems with entrance channel mass asymmetry lower than the Businaro–Gallone critical mass asymmetry,[4] mass flow occurs from heavier to lighter reaction partner and the composite system moves towards symmetry on the potential energy surface. The direction of mass flow is reversed if entrance channel mass asymmetry is greater than Businaro–Gallone critical mass asymmetry. Mathews *et al.*[5] reported growth of the projectile at the expense of target in ^{20}Ne+$^{\text{nat}}$Cu and ^{20}Ne+^{197}Au reactions. Contribution from these various processes depends on the projectile energy and entrance channel mass asymmetry. In reactions involving light projectiles such as ^{12}C, ^{16}O, ^{19}F and ^{20}Ne on various targets, ICF and QET reactions are observed as the dominant noncompound processes in the beam energy range below $\sim$6 MeV/nucleon.[3,6–13]

In reaction systems with comparatively lower entrance channel mass asymmetry, such studies are limited. D′Erasmo *et al.*[14] measured the elemental yield of PLFs as a function of total kinetic energy loss (TKEL) in ^{32}S+^{92}Mo, ^{32}S+^{93}Nb and ^{28}Si+^{93}Nb reactions at beam energies corresponding to the $E_{\text{cm}}/V_{\text{c}}$ value of about $\sim$1.4, where E_{cm} and V_{c} are projectile energy and entrance channel Coulomb barrier in the centre of mass frame of reference. These studies showed increasing N/Z equilibration with increasing TKEL i.e., with increasing kinetic energy dissipation. Measurement of cross section of reaction products in ^{16}O+^{66}Zn and ^{37}Cl+^{45}Sc showed much larger cross section for QET and ICF reactions in ^{16}O+^{66}Zn reaction compared to that in ^{37}Cl+^{45}Sc reactions.[13] Beam energy for ^{37}Cl+^{45}Sc reaction in this study was below $\sim$3.5 MeV/nucleon. It would be important to investigate the contribution from different processes involving incomplete mass transfer in systems with low entrance channel mass asymmetry at higher beam energies to get information about the magnitude and types of mechanisms involved. Also the composite system mass for these reactions is close to the mass region $\sim$100 which is the transition region where behaviour of liquid drop potential energy as a function of mass asymmetry is reversed.[4] Such reactions may also have contribution from

fission, arising mainly from the large l-waves, which lead to a preferential lowering of the fission barrier for symmetric split.[15]

In the present work, reaction products formed in complete fusion and incomplete mass transfer processes have been measured in ^{28}Si+^{93}Nb reaction at $E_{\rm lab} = 105$ and 155 MeV by recoil catcher technique followed by off-line γ-ray spectrometry to investigate the contribution from different mechanisms contributing to incomplete mass transfer.

2. Experimental Details

Experiments were carried out at BARC-TIFR Pelletron–LINAC facility, Mumbai. Self supporting targets of ^{93}Nb (Thickness: 2.1 mg/cm^2) were irradiated with ^{28}Si beam at beam energies of 110 and 160 MeV. Average energies at the center of the target were 105 and 155 MeV, respectively due to the beam energy degradation in the target. A schematic of target catcher assembly is shown in Fig. 1. Two aluminium catcher foils were kept in the forward direction to stop the reaction products recoiling in the forward hemisphere. The thickness of first catcher (catcher 1) foil was about 700 μg/cm^2 and that of the second catcher foil was 6.75 mg/cm^2. This 'double catcher arrangement' avoided the contribution from the products of ^{28}Si+^{27}Al reaction in the gamma-ray spectrum of the first catcher foil. In the backward direction, an aluminium foil of thickness 6.75 mg/cm^2 was arranged in a conical geometry (with a 5 mm diameter hole in the centre for the passage of the beam) to clearly identify fission products if formed. Irradiations were carried out for about 9 and 7 h at lower and higher beam energies, respectively. After irradiation, target and catcher foils were separately counted for the γ-rays of the reaction products using a HPGe detector coupled to a multichannel analyzer. The shortest cooling time before start of counting was about $\sim$7 min. Repeated counting of samples was continued for more than three months to obtain the cross sections of reaction products having half-life in the range of few minutes to months. Various reaction products were identified by matching their half-lives and gamma-ray energies.

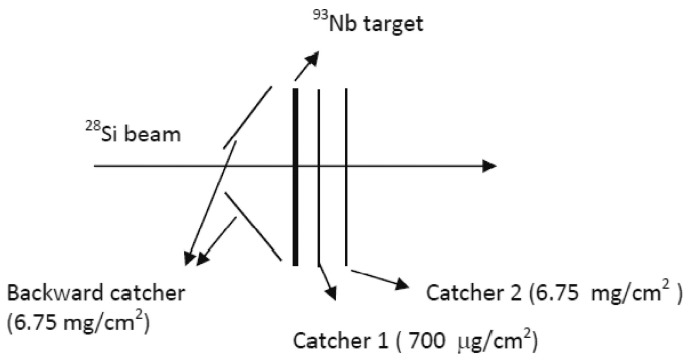

Fig. 1. Schematic of target catcher irradiation assembly.

3. Results and Discussion

Typical γ-ray spectra of targets and the first catcher foils are shown in Figs. 2 and 3, respectively. Gamma-ray spectrum for $E_{\rm lab} = 105$ and 155 MeV are shown as dotted and solid lines, respectively. All the spectra correspond to a cooling of about three days and were acquired for 5000 s. From the γ-ray spectra, several reaction products with atomic number in the range of 39–54 were identified. Gamma-rays due to the fission products were not observed in any of the catcher foils. Gamma-rays of some of the reaction products are marked in the spectra. Gamma-ray spectrum of the backward catcher foil is not shown as none of the products from ^{28}Si+^{93}Nb reaction was observed. Gamma-ray spectra were analyzed using peak area analysis software PHAST[16] to obtain the peak areas for characteristic gamma-rays of various reaction products. From the peak area, 'end of irradiation' activity of a given reaction

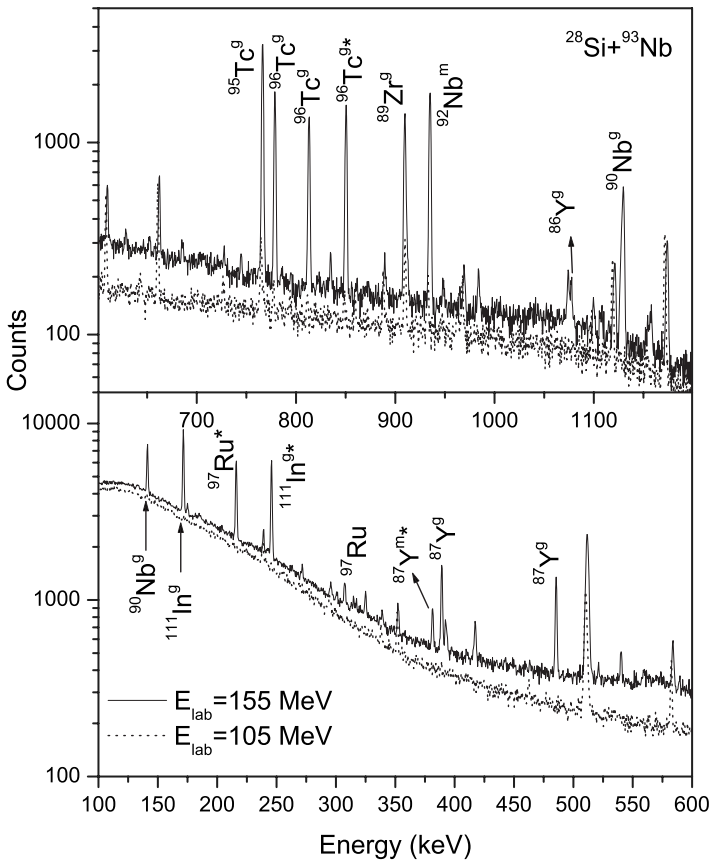

Fig. 2. Gamma-ray spectra of the target at $E_{\rm lab} = 155$ MeV (solid line) and at 105 MeV (dotted line). Gamma-rays due to different reaction products are marked in the figure. Cooling time before the start of counting is about three days and counting time is 5000 s. In the case of multiple prominent gamma-rays for a given product, the gamma-ray used for the cross section calculation has been marked by asterisk (*).

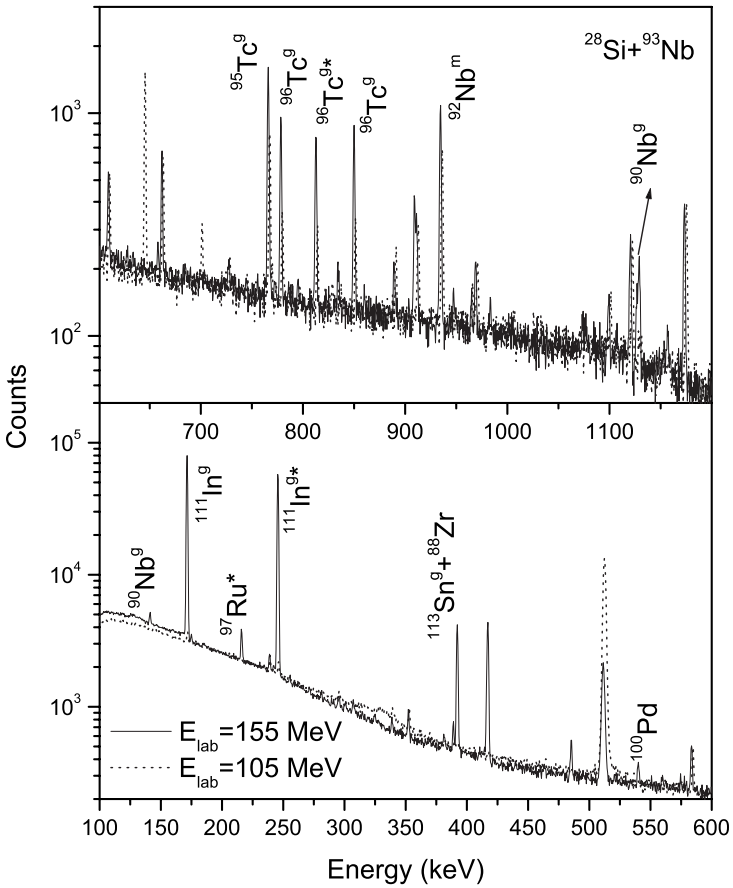

Fig. 3. Same as Fig. 2, for the first catcher foil.

product was obtained using the following equation

$$A(dps) = \frac{P_A \frac{\mathrm{CT}}{\mathrm{LT}}}{(e^{-\lambda T_{\mathrm{cool}}})[(1-e^{-\lambda \mathrm{CT}})/\lambda](a_\gamma/100)\varepsilon(E_\gamma)}, \quad (1)$$

where P_{A} is the peak area under a characteristic gamma-ray peak, CT and LT are the clock (Real) and live time of the data acquisition system respectively, T_{cool} is the time elapsed after irradiation till start of the spectrum acquisition, λ is the decay constant of the radionuclide, a_γ is the gamma-ray abundance and ε is the full energy detection efficiency for the gamma-ray of energy E_γ. Decay data of evaporation residues (ERs) such as half-life ($T_{1/2}$), gamma-ray energy (E_γ) and γ-ray abundance (a_γ) were taken from Refs. 17 and 18 and are given in Table 1. It can be seen from the table that gamma-ray energies of ^{116}Te (931.8 keV) and ^{92}Nb$^{\mathrm{m}}$(934.5 keV) are close. However, these gamma-rays could be resolved by the detector so that the peak areas for the two gamma-ray peaks could be obtained

using the peak area analysis software PHAST.[16] The end of irradiation activity (A) of a reaction product was used to calculate its formation cross section using the following equation

$$\sigma = \frac{A}{N\sum_{i=1}^{n}\phi_i(1-e^{-\lambda\Delta T_{\rm irr}})e^{-\lambda(T_{\rm irr}-i\Delta T_{\rm irr})}}, \tag{2}$$

where N is number of target atoms per unit area, $\phi_{\rm i}$ is the number of beam particles incident on the target per unit time in the ith time interval, $\Delta T_{\rm irr}$ is the duration of time interval, n is the total number of intervals and $T_{\rm irr}(= n \times \Delta T_{\rm irr})$ is the total irradiation time. Beam current was recorded for small time intervals to take care of the fluctuation in the beam intensity during irradiation. From the electrical current (I), number of beam particles incident on the target per unit time was determined as $\mathrm{I}/(q \times 1.602 \times 10^{-19})$, where q is the charge state of the beam particles which was estimated using the prescription from Ref. 19. The average charge states at $E_{\rm lab} = 105$ and 155 MeV were calculated as 10 and 10.8, respectively.

Formation cross sections of reaction products in ^{28}Si+^{93}Nb reaction at $E_{\rm lab} =$ 105 and 155 MeV are given in Table 1. Cross sections given in Table 1 are sum of the cross sections of respective ERs in the target and different catcher foils. Uncertainties quoted on the cross sections are standard deviation of the cross sections or propagated error on the peak areas obtained from multiple rounds of counting, whichever is higher. An upper limit of the uncertainty due to the other sources such as efficiency, charge state of the beam particles and target thickness was estimated to be around 20%. For many radionuclides which are expected to have contribution from the precursor decay, independent cross section of the daughter $\sigma_d^{\rm ind.}$ was obtained using the equation[20]

$$\sigma_d^{\rm ind} = \sigma_d^{\rm cumm.} - \frac{\lambda_d}{\lambda_d - \lambda_p}\sigma_p, \tag{3}$$

where $\sigma_d^{\rm cumm}$ is the experimental cumulative cross section of the daughter nucleus and $\sigma_{\rm p}$ is the experimental cross section of the parent (precursor) which may be cumulative or independent. $\lambda_{\rm d}$ and $\lambda_{\rm p}$ are the decay constants of the daughter and the parent (precursor), respectively. The symbol 'I' and 'C' represent independent and cumulative cross sections, respectively. For the cases where it was not possible to confirm whether the yield is 'independent' or 'cumulative' it has not been specified in the table. A comparison of the cross sections of the products around the target mass ($A_{\rm T} = 93$) at the two beam energies shows that the contribution from incomplete mass transfer processes is much higher at $E_{\rm lab} = 155$ MeV compared to that at 105 MeV. This can be correlated to the population of large number of l-waves above critical angular momentum for complete fusion ($l_{\rm crit}$) at $E_{\rm lab} = 155$ MeV. The values of maximum angular momentum ($l_{\rm max}$) and critical angular momentum $l_{\rm crit}$, calculated using the prescription of Ref. 21 are given in Table 2. As seen from Table 2, $l_{\rm max}$ value is much lower compared to $l_{\rm crit}$ at $E_{\rm lab} = 105$ MeV, whereas it

Table 1. Cross sections of reaction products formed in ^{28}Si+^{93}Nb reaction at $E_{\rm lab} = 155$ MeV and 105 MeV. Nuclear data of evaporation residues such as half-life ($T_{1/2}$), gamma-ray energy (E_γ) and gamma-ray abundance (a_γ) have been taken from Refs. 17 and 18. 'I' and 'C' denote independent and cumulative cross sections, respectively. Cross sections given in the table are sum of the cross sections in the target and catcher foils.

				Cross section (mb)	
Isotope	$T_{1/2}$	E_γ (keV)	a_γ(%)	$E_{\rm lab} = 155$ MeV	$E_{\rm lab} = 105$ MeV
^{86}Y^{g}	14.74 h	1076.3	82.5	1.27 ± 0.20 (I)	
^{87}Y^{m}	12.9 h	381.1	78.1	3.10 ± 0.39 (I)	
^{88}Zr	83.4 d	392.9	97.3	3.41 ± 0.26	
^{89}Zr^{g}	3.27 d	909.2	99	9.04 ± 0.29	
^{90}Nb^{g}	14.6 h	1129.1	92	12.46 ± 0.32 (I)	0.21 ± 0.02 (I)
^{92}Nb^{m}	10.15 d	934.5	99	33.5 ± 0.6 (I)	13.2 ± 0.3 (I)
^{93}Mo^{m}	6.85 h	684.7	99.7	11.2 ± 0.6 (I)	0.221 ± 0.046 (I)
^{93}Tc^{g}	2.75 h	1362.9	66.2	5.25 ± 0.35	
^{94}Tc^{g}	293 min	702.7	99.6	16.0 ± 0.5 (I)	0.99 ± 0.19 (I)
^{95}Tc^{g}	20.0 h	765.8	93.9	27.2 ± 0.7 (I)	6.22 ± 0.22 (I)
^{95}Tc^{m}	61.0 d	204.1	66.5	2.77 ± 0.30 (I)	
^{95}Ru	1.643 h	336.4	70.2	1.56 ± 0.10 (I)	
^{96}Tc^{g}	4.28 d	849.9	97.8	13.0 ± 1.4 (I)	1.94 ± 0.11 (I)
^{97}Rh^{g}	31.1 min	421.5	75	0.65 ± 0.25	
^{97}Ru	2.9 d	215.7	85.8	7.13 ± 0.44 (I)	0.123 ± 0.023
^{100}Pd	3.63 d	539.6	103	0.29 ± 0.05 (I)	
^{101}Rh^{m}	4.34 d	306.9	86.3	1.38 ± 0.13 (I)	
^{108}In^{m}	58.0 min	242.9	37	9.9 ± 1.0 (I)	
^{109}In	4.2 h	203.5	203.5	26.4 ± 0.9 (I)	
^{110}In	4.9 h	657.8	98.3	89 ± 9 (I)	
^{111}In^{g}	2.63 d	245.4	94	99 ± 6	0.86 ± 0.11
^{113}Sn^{g}	115.1 d	391.7	64	293 ± 6 (C)	
^{114}Te	15.2 min	1299.9	127.8	102 ± 3	8.47 ± 0.35
^{115}Sb	32.1 min	497.3	98.2	126 ± 2	61 ± 1
^{116}Te	2.49 h	931.8	27.7	198 ± 6	10.3 ± 0.6
^{117}Te	1.03 h	719.7	64.7	77 ± 3	82 ± 3
^{118}I(2−)	13.7 min	605.6	86.01	4.6 ± 1.2	204 ± 11 (I)
^{118}I(7−)	8.5 min	614.3	64.98		10.8 ± 0.7 (I)
^{118}Xe	6 min	274	30		13 ± 5
^{119}I	19.1 min	257.5	86.7		19.9 ± 1.5 (I)
^{119}Xe	5.8 min	461.5	91		3.07 ± 0.61

is substantially above $l_{\rm crit}$ at $E_{\rm lab} = 155$ MeV. It can be seen from the table that processes involving transfer of only a few nucleons occur even at the lower energy. This is consistent with the fact that QET reactions compete with complete fusion even at beam energies close to the entrance channel Coulomb barrier. This was also observed in our earlier measurements of cross sections of PLFs in ^{19}F+^{89}Y,^{66}Zn reactions as a function of beam energy.[8,9] These measurements showed that the cross sections of lighter PLFs formed in massive transfer reactions fall more rapidly with decreasing beam energy compared to those of the heavier PLFs.[8,9] It is important to note that a substantial part of the relative angular momentum gets converted into spin angular momentum even for reactions involving exchange of only a few

nucleons. For example, formation of ^{93}Mo$^{m}(21/2^{+})$ in large yields which involves proton–neutron exchange between the projectile and the target nucleus. Similarly, ^{95}Tc which is expected to be formed in ^{4}He transfer channel, formation of high spin $(9/2^{+})$ isomer is about ∼10 times higher compared to that of the low spin isomer $(1/2^{-})$ at $E_{\rm lab} = 155$ MeV.

Cross sections of different reaction products in a given mass chain were added to obtain mass yields which are shown in Figs. 4(a) and 4(b) for $E_{\rm lab} = 105$ and 155 MeV, respectively. For comparison, mass yields calculated using the statistical model code PACE2[22] for compound nucleus de-excitation is also shown in the figure. PACE2 calculations were carried out with default set of parameters with the level density parameter 'a' taken as $A/9$ MeV^{-1}. The total experimental fusion cross section at $E_{\rm lab} = 105$ MeV, obtained by adding the cross sections of ERs with $A > 100$ was 413 ± 13 mb. This mass cut-off was chosen as evaporation followed by complete fusion is not expected to populate masses lower than 100. Experimental fusion cross section was substantially larger compared to the complete fusion cross section based on Bass model[23] as used in PACE2 code.[22] Therefore, in the PACE2 calculations at $E_{\rm lab} = 105$ MeV, total fusion cross section of 413 mb was supplied as input. It can be seen from Fig. 4(a) that PACE2 calculations are in reasonable agreement with the experimental cross sections of reaction products at $E_{\rm lab} = 105$ MeV ($E^{*}_{\rm cn} = 49.1$ MeV, where $E^{*}_{\rm cn}$ is the compound nucleus excitation energy). At $E_{\rm lab} = 155$ MeV ($E^{*}_{\rm cn} = 87.5$ MeV), a tendency of more neutron evaporation populating lower masses was observed in the calculations as seen in Fig. 4(b). The total experimental fusion cross section at $E_{\rm lab} = 155$ MeV was 1025 ± 15 mb which was lower compared to the total fusion cross section calculated using the PACE2 code as 1164 mb. This is due to the fact that some of the reaction products e.g., reaction products in mass chain with $A = 112$ could not be measured due to their unsuitable decay characteristics. In fact, the actual difference between the experimental and calculated total fusion cross sections will be more as experimental fusion cross section will have the contribution from massive transfer or ICF reaction which would also form reaction products with similar masses as those formed in complete fusion.

The total experimental reaction cross sections, obtained by adding cross sections of all the reaction products, at the two beam energies are compared with the reaction cross sections calculated using the sum-rule model[24,25] in Table 2. At lower beam energy experimental reaction cross section is close to calculated value.

Table 2. Maximum angular momentum ($l_{\rm max}$) and critical angular momentum ($l_{\rm crit}$) along with experimental and calculated reaction cross sections (using sum-rule model[24,25]) for ^{28}Si+^{93}Nb reaction at $E_{\rm lab} = 105$ and 155 MeV.

$E_{\rm lab}$ (MeV)	$l_{\rm max}$ ($\hbar$)	$l_{\rm cirt}$ ($\hbar$)	$\sigma_{R,\rm exp}$ (mb)	$\sigma_{R,\rm calc}$ (mb)
105	33	52	436 ± 14	425
155	78		1175 ± 20	1600

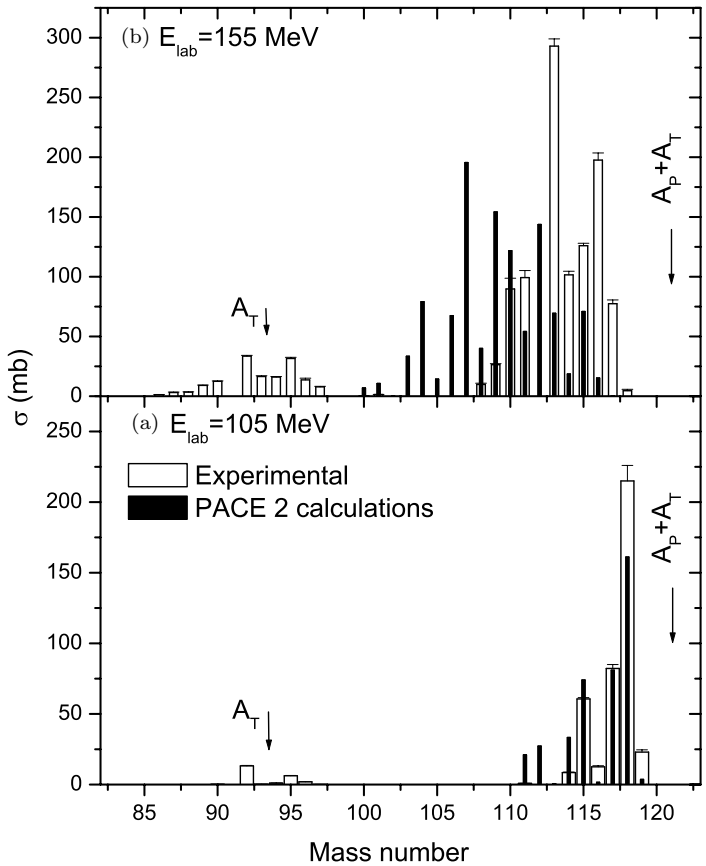

Fig. 4. Comparison of calculated and experimental cross sections for different mass chains at $E_{\rm lab} = 105\,\rm MeV$ (a) and $E_{\rm lab} = 155\,\rm MeV$. (b) A_P and A_T are projectile and target masses, respectively.

Experimental cross sections of reaction products around the target mass shows that the contribution from QET at this beam energy is of the order of ∼5%. Based on sum-rule model, contribution from incomplete mass transfer processes is expected to be significant only at beam energies, for which $l_{\rm max} > l_{\rm crit}$. At $E_{\rm lab} = 155\,\rm MeV$, the expected contribution from incomplete mass transfer processes is 27% based on the difference between complete fusion cross section, calculated using PACE2 code, and reaction cross section calculated using sum-rule model.[24,25] Cross sections of reaction products centered around target mass, which are purely formed in QET and DIC (as no contribution from compound nucleus evaporation is expected in this mass region) account for about ∼9%. A part of the remaining cross section would be present as massive transfer or ICF reaction forming reaction products similar to those formed in complete fusion. An approximate estimate of the yield of the massive or ICF products having mass close to those of complete fusion products can be obtained from the prompt mass (before particle evaporation) yields

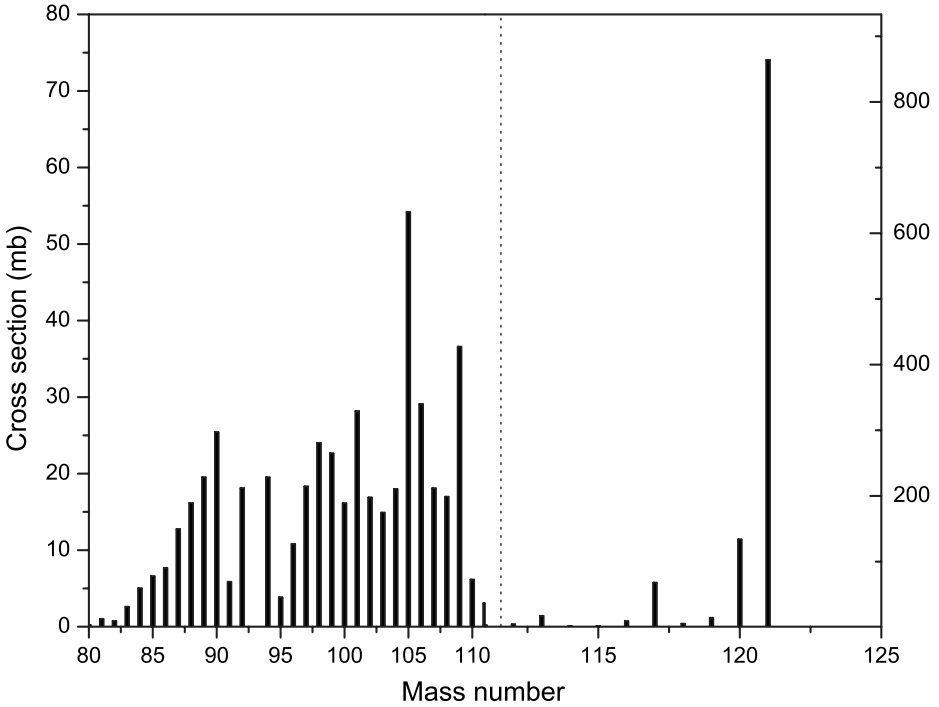

Fig. 5. Plot of prompt mass yields calculated using sum-rule model for ^{28}Si+^{93}Nb reaction at $E_{\rm lab} = 155$ MeV. The dotted line in the figure marks the change in the scale of X and Y-axes.

calculated using sum-rule model as shown in Fig. 5. The dotted line in the figure marks the change in the scale of X and Y-axes. Substantial cross section for the products formed in incomplete mass transfer processes is predicted in addition to complete fusion ($A = 121$). It can be seen from this figure that the ICF product with $A = 117$, formed in ^{24}Mg transfer, is predicted to be formed in good yield in sum-rule calculations. Assuming that the outgoing part of the projectile goes away with the beam velocity, beam energy can be apportioned between the transferred fragment ^{24}Mg and outgoing part of the projectile ^{4}He in their mass ratio. Based on this assumption, the recoil energy of the product with $A = 117$ was estimated assuming collision of ^{24}Mg fragment with the target nucleus with energy ($E_{\rm F}$) equal to (24/28)*$E_{\rm lab}$ which was lower by about 8 MeV compared to the recoil energy of the compound nucleus. This difference is large enough to be reflected in the fraction of the reactions products reaching the forward catcher foils. The excitation energy of the ICF product formed in ^{24}Mg transfer i.e., ^{117}I was estimated using $E_{\rm F}$ as 75 MeV which suggests formation of reaction products in the mass region around ∼109 after particle evaporation, assuming the loss of about ∼9 MeV per neutron. In the plot of fractional yields of reaction products in the forward catcher foils as a function of their mass number (Fig. 6), a drop around $A \sim 109$ due to the partial linear momentum transfer can be seen. A decrease in the fractional yield

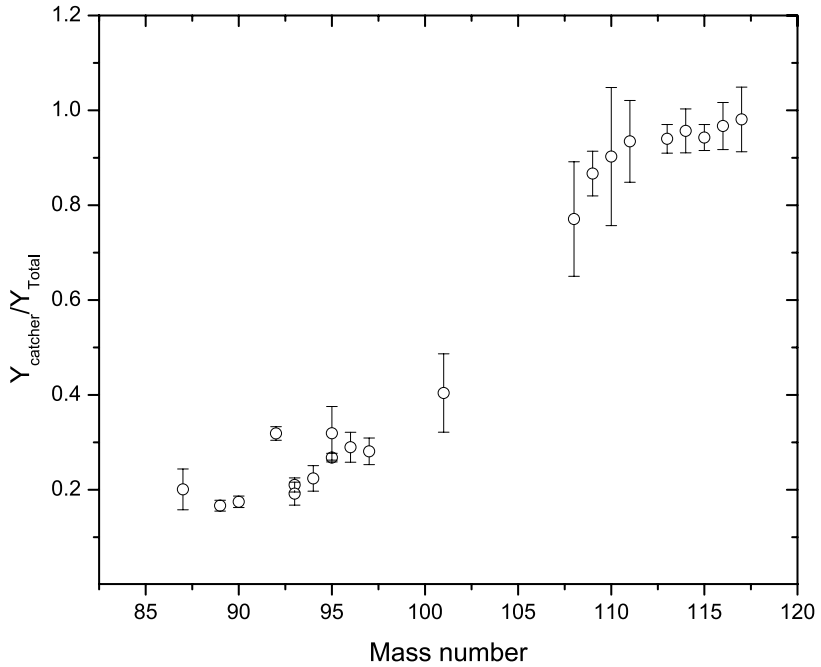

Fig. 6. Plot of fractional yield of reaction products in the catcher foil at $E_{\rm lab} = 155\,$MeV.

with decreasing mass of the reaction products shows decreasing linear momentum transfer. In the higher mass region, the fractional yield attains a maximum value of around unity indicating complete fusion to be the dominant mechanism. Based on sum-rule model calculations, contribution from ^{24}Mg transfer, which is the dominant transfer channel forming reaction products in the intermediate mass region, is about 4.2% of the reaction cross section. Sum-rule calculations are also consistent with the experimental observation of products in two groups as seen in Fig. 5, though these yields are centered at comparatively higher masses as being prompt mass yields. Such a separation was also consistent with the experimental distribution pattern of reaction products in the target and the two catcher foils. Assuming all the prompt masses with $A \leq 110$ to form products with $A < 100$, the products centered around the target mass should account for about 14% of the reaction cross section. The experimental value is 9.3%. Thus, sum-rule calculations slightly overestimate the cross section in the lighter mass region.

Experimental mass yields of reaction products close to the target mass are plotted again for $E_{\rm lab} = 155\,$MeV in Fig. 7. As seen from the figure, the distribution is peaked close to the target mass and extending (towards lower mass region) up to $A = 86$ corresponding to the stripping of seven nucleons. Towards the higher mass region the distribution is extended up to $A = 101$ corresponding to the pick-up of eight nucleons. Nearly symmetric distribution of mass yields around the target mass shows contribution from DIC in addition to QET. The direction of the mass

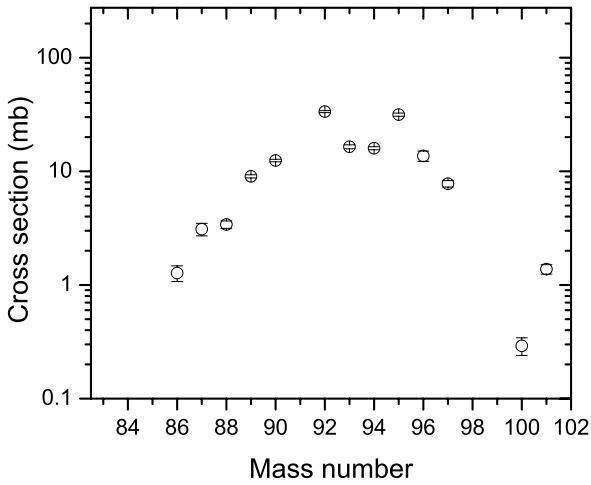

Fig. 7. Plot of mass yields close to the target mass at $E_{\rm lab} = 155\,\rm MeV$.

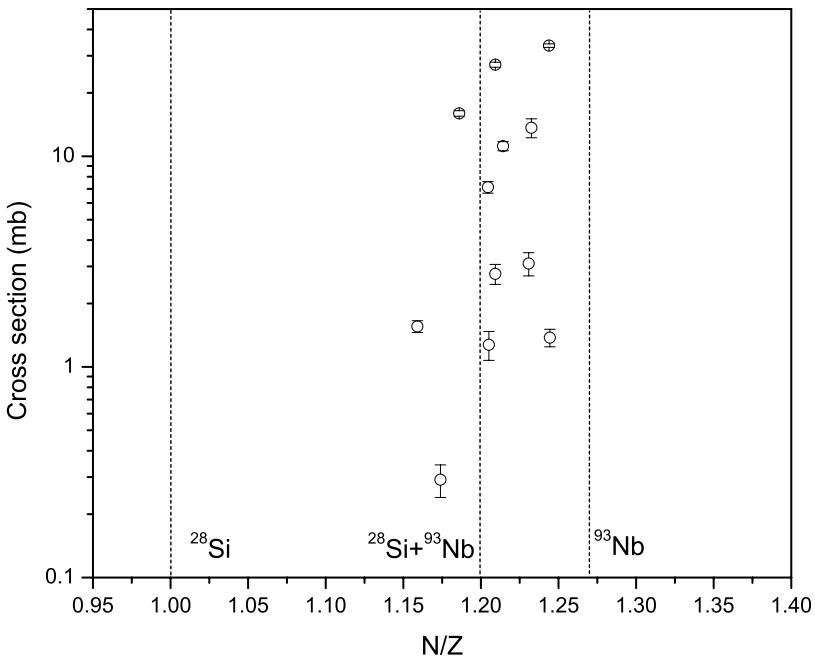

Fig. 8. Plot of independent cross sections of evaporation residues in the vicinity of target mass as a function of their $N/\rm Z$ values at $E_{\rm lab} = 155\,\rm MeV$.

flow depends on the value of entrance channel mass asymmetry relative to the Businaro–Gallone critical mass asymmetry.[4] D'Erasmo *et al.*[14] measured elemental distribution of PLFs gated with TKEL in ^{28}Si+^{93}Nb reaction at $E_{\rm lab} = 140\,\rm MeV$. In this study, it was shown that the mean value of Z of the PLFs moves closer to

that corresponding to N/Z of the equilibrated system with increasing TKEL. In the order to investigate N/Z equilibration in the present work, independent cross sections of reaction products around target mass are plotted as a function of their N/Z in Fig. 8. Dotted lines corresponding to N/Z of ^{28}Si (projectile), ^{93}Nb (target) and ^{28}Si+^{93}Nb (composite system) are also marked in the figure. It can be seen from the figure that, these products are distributed above as well as below the composite system N/Z indicating contribution from transfer and pick-up reactions of quasi-elastic nature as well as DIC mechanism. Products with N/Z close to that of the target would be predominantly formed in QET reactions whereas those around composite system would be mainly formed in DIC. It should be mentioned here that ERs having masses less than the target mass were not observed in earlier measurement in ^{37}Cl+^{45}Sc reaction.[13] Maximum energy for measurement in ^{37}Cl+^{45}Sc reaction[13] was 124 MeV ($E_{\rm cm}/V_{\rm c} = 1.31$) which is lower compared to the beam energy of 155 MeV ($E_{\rm cm}/V_{\rm c} = 1.57$) of the present study. This observation suggests the role of beam energy relative to the entrance channel Coulomb barrier in governing the contribution from DIC and pick-up reactions, which in turn, leads to the population of large number of l-waves above $l_{\rm crit}$. Thus, in the reaction with heavy projectiles at sufficiently high beam energy, DIC is also observed in addition to QET and ICF reactions. This behavior is different from that observed in reactions involving lighter projectiles ($A <\sim 16$), for which QET and ICF reactions, involving mass transfer from projectile to target, dominate even at higher beam energy.

4. Conclusions

Measurement of cross sections of reaction products in ^{28}Si+^{93}Nb reaction at $E_{\rm lab} = 105$ and 155 MeV showed substantial contribution from incomplete mass transfer processes at higher beam energy. Products could be broadly divided into two groups, one centered around the target mass and other below the 'projectile ($A_{\rm P}$)+target($A_{\rm T}$)' mass. These studies showed that reactions involving heavy projectiles have substantial contribution from DIC in addition to QET and massive transfer or ICF reactions. This was also confirmed by the analysis of N/Z values of the reaction products. This observation is different from the reactions involving lighter projectiles ($A <\sim 16$) where transfer predominantly occurs from projectile to target. These results show that, in the beam energy range of $\sim$6 MeV/nucleon, mass transfer from lighter to heavier reaction partner occurs for reaction systems with lower entrance channel mass asymmetry, thereby, implying the importance of entrance channel mass asymmetry in governing the reaction mechanism. At $E_{\rm lab} = 105$ MeV, the reaction mechanism was observed to be exclusively fusion-evaporation except for small contribution from QET.

Acknowledgments

We thank Dr. K. Sudarshan for fruitful discussion. We thank the staff of BARC-TIFR Pelletron-Linac facility, Mumbai for smooth operation.

References

1. L. Corradi, G. Pollarolo and S. Szilner, *J. Phys. G* **36** (2009) 113101.
2. B. S. Tomar, A. Goswami, G. K. Gubbi, A. V. R. Reddy, S. B. Manohar, B. John and S. K. Kataria, *Phys. Rev. C* **58** (1998) 3478.
3. J. Galin, B. Gatty, D. Guerreau, M. Lefort, X. Tarrago, S. Agarwal, R. Babinet, B. Cauvin, J. Girard and H. Nifenecker, *Z. Phys. A* **283** (1977) 173.
4. U. L. Businaro and S. Gallone, *Nuovo Cimento* **5** (1957) 315; K. T. R. Davies and A. J. Sierk, *Phys. Rev. C* **31** (1985) 915.
5. G. J. Mathews, J. B. Moulton, G. J. Wozniak, B. Cauvin, R. P. Schmitt, J. S. Sventek and L. G. Moretto, *Phys. Rev. C* **25** (1982) 300.
6. A. Yadav, V. R. Sharma, R. Kumar, P. P. Singh, D. P. Singh, Unnati, M. K. Sharma, B. P. Singh and R. Prasad, *Phys. Rev. C* **86** (2012) 014603.
7. D. Singh, R. Ali, M. Afzal Ansari, M. H. Rashid, R. Guin and S. K. Das, *Nucl. Phys. A* **879** (2012) 107.
8. R. Tripathi, K. Sudarshan, S. Sodaye, A. V. R. Reddy, A. Goswami, B. K. Nayak and S. K. Sharma, *Phys. Rev. C* **79** (2009) 064604.
9. R. Tripathi, K. Sudarshan, S. Sodaye and A. Goswami, *J. Phys. G.* **35** (2008) 025101.
10. R. Tripathi, S. Sodaye, K. Mahata and P. K. Pujari, *Phys. Rev. C* **90** (2014) 027604.
11. Amit Kumar, R. Tripathi, S. Sodaye, K. Sudarshan and P. K. Pujari, *Eur. Phys. J A* **49** (2013) 1.
12. K. Surendra Babu, R. Tripathi, K. Sudarshan, B. D. Srivastava, A. Goswami and B. S. Tomar, *J. Phys. G* **29** (2003) 1011.
13. S. Sodaye, B. S. Tomar and A. Goswami, *Pramana J. Phys.* **66** (2006) 985.
14. G. D'Erasmo *et al.*, *Z. Phys. A* **321** (1985) 425.
15. Y. Nagame, H. Ikezoe and T. Ohtsuki, *Phys. Rev. C* **47** (1993) 1586.
16. P. K. Mukhopadhyaya, in *Proc. DAE Symp. Intelligent Nuclear Instrumentation* (*INIT-2001*), eds. by S. K. Kataria, P. P. Vaidya, P. V. Narurkar and S. Roy (BARC, Mumbai, India, 2001), p. 307.
17. R. B. Firestone and V. S. Shirley, *Table of Isotopes*, 8th edn. (Wiley-Inter Science Publication, New York, 1999).
18. U. Reus and W. Westmeier, *At. Data Nucl. Data Tab.* **29** (1983) 1.
19. H. D. Betz, *Rev. Mod. Phys.* **44** (1972) 465; L. C. Northcliffe, *Ann. Rev. Nucl. Sci.* **13** (1963) 67.
20. M. Cavinato, E. Fabrici, E. Gadioli, E. Gadioli Erba, P. Vergani, M. Crippa, G. Colombo, I. Redaelli and M. Ripamonti, *Phys. Rev. C* **52** (1995) 2577.
21. J. Wilczynski, *Nucl. Phys. A* **216** (1973) 386.
22. A. Gavron, *Phys. Rev. C* **21** (1980) 230.
23. R. Bass, *Phys. Rev. Lett.* **39** (1977) 265.
24. J. Wilczynski, K. Siwek-Wilczynska, J. Van Driel, S. Gonggrijp, D. C. J. M. Hageman, R. V. F. Janssens, J. Lukasiak, R. H. Siemssen and S. Y. Van Der Werf, *Nucl. Phys. A* **73** (1982) 109.
25. K. Siwek-Wilczynska, E. H. du Marchie van Voorthuysen, J. van Popta, R. H. Siemssen and J. Wilczynski, *Phys. Rev. Lett.* **42** (1979) 1599.